Mining of Mineral Deposits
Volume 20 (2026), Issue 1, 59-70

MMD JOURNAL / MINING.IN.UA

https://doi.org/10.33271/mining20.01.059

Research into fracture mechanism of complex-structured crystalline mass under triaxial compression

Oleksii Ishchenko [1], Leonid Novikov [2], Ivan Ponomarenko [3], Volodymyr Konoval [3], Roman Kinasz [4], Kostiantyn Ishchenko [2*]

[1] *Dnipro University of Technology, Dnipro, Ukraine*
[2] *M.S. Poliakov Institute of Geotechnical Mechanics of the National Academy of Sciences of Ukraine, Dnipro, Ukraine*
[3] *Cherkasy State Technological University, Cherkasy, Ukraine*
[4] *AGH University of Science and Technology, Krakow, Poland*

**Corresponding author: e-mail ishenko_k@i.ua*

Abstract

Purpose. The research aims to use experimental and theoretical studies in assessing the nature of fracture of cracked crystalline mass samples with a complex structure in the brittle-plastic area under the action of triaxial loading.

Methods. To assess the influence of physical-mechanical properties of a cracked crystalline mass and its structural peculiarities on the change in the nature of its fracture, experimental studies were conducted on rock samples. Samples were taken from the faces of preparatory workings in uranium mines, tunnels of the subway under construction (the city of Dnipro) and from the benches of granite quarries in Ukraine. The tests were conducted using proven methods in accordance with current government standards. During the testing process, the samples and the nature of crack formation were assessed synchronously using a GAOSUO P scanning microscope, and their characteristics were assessed using acoustic emission (AE) method and CT-scanning with an industrial Micro-CT scanner, the results of which were processed using Avizo software.

Findings. During testing of the samples, it was found that their uniaxial compressive strength and fracture mode are similar. Tests have revealed several types of crack inclination angles depending on bedding. With an increase in the value of σ_3, the values of σ_{1p} and σ_d increase almost linearly, while the values of σ_{1p} and σ_d of the samples first decrease, and then increase with an increase in the β value. It was revealed that between the crack opening and the stress state of the crack surfaces at stresses σ_1 and σ_2, additional strain of the sample is formed exclusively in the direction of σ_3.

Originality. It was determined that during testing of samples, the value of σ_3 has a significant influence on the "stress-strain" curve characteristics with different values of β. Then, an increase in σ_3, σ_1-σ_3, ε_1, ε_3, ε_v values indicates the ability to resist external loads and strains when testing cracked rock samples. It was proven that when σ_3 is low, the linear elastic component in the "stress-strain" curve section has a greater proportion than in the yield curve section with an increase of σ_3.

Practical implications. The research conducted served as a basis for further development of theory and methods in fracture mechanics of cracked (stratified) crystalline mass, disaster prediction during mining operations in the construction of mine workings and tunnels at mining enterprises.

Keywords: *rock; triaxial load system; crystalline mass; acoustic emission; CT-scanning; differential stresses*

1. Introduction

Increase in the volume of constructing underground structures and large-section workings (main line tunnels on railways and subways in cities, mine workings in deep mines and quarries), especially in difficult mining-geological conditions [1]-[3], ensuring the stability of bench slopes during mineral extraction in quarries [4], [5], mining of coal [6], [7] and shale gas [8], [9] in conditions of crystalline rock mass with a complex structure – all require the improvement of existing and development of new resource-saving technological solutions for fracturing and processing of minerals with surface and underground cycles of operations.

The results showed that complex-structured crystalline masses differ from structurally homogeneous rock masses by a marked natural anisotropy of physical-mechanical properties, the presence of both vertical and horizontal crack systems of varying intensity, with alternating sections of highly cracked and almost monolithic strong rock. It was determined that the existing bedding planes with varying bedding angles in them have a significant influence on their mechanical characteristics, crack propagation, and fracture conditions. In this case, the horizontal-stratified rock mass is also characterized by transverse isotropy, within which there are structurally weakened complex-structured planes, both paral-

Received: 28 September 2025. Accepted: 24 February 2026. Available online: 30 March 2026

Mining of Mineral Deposits. ISSN 2415-3443 (Online) | ISSN 2415-3435 (Print)

lel to the structural plane and perpendicular to it, alternating with soft and hard layers. In addition, in its natural state, such a rock mass has many cracks, which leads to its characteristic anisotropy under the action of forces and strains [10]-[13]. Therefore, it is very important to study the influence of the angles and direction of crack propagation (bedding) on the anisotropic behaviour of a complex-structured crystalline (stratified, cracked) mass.

Due to the intensive mining of minerals occurring close to the surface, their reserves were depleted, prompting further development of underground mining at deeper levels [14]-[16]. As the depth of mining increases, the stress-strain state (SSS) of the rock gradually changes from brittle to plastic behaviour [17], [18]. Therefore, experimental and theoretical studies limited to a fragile area are insufficient to meet the needs of deep-horizon mining technologies [19]. Furthermore, numerous in-situ stress measurements demonstrated that the SSS in surrounding stratified cracked, complex-structured rocks at great depth exhibits significant three-dimensional (3D) anisotropy, commonly referred to as true triaxial stress state [20]-[22].

With the creation of new digital experimental equipment, research methods, computer data processing technologies, numerous tests were conducted on true triaxial compression to study the mechanical behaviour of various rocks, such as sandstone [23]-[27], slate [28], marble [29]-[31], granite [32]-[34], coal [35], [36], concrete [37], [38] and cement stone [19], [20]. Under true triaxial loading, rocks exhibit stress-induced anisotropy and their response to "stress-strain" [19], [20], [39]. As the intermediate principal stress increases, the corresponding strain changes from tension to compression. In addition, both the intermediate principal stress and hydrostatic pressure influence the three-level path of principal strains in space [20]. The true triaxial strength characteristics are explained by a non-monotonic initial increase, followed by a decrease in them as the intermediate principal stress increases [21]-[23]. Strength is closely related to stress state parameters [22], including intermediate principal stress, the Noda-Lode parameter (coefficient) [40], and hydrostatic pressure.

In recent years, domestic [41]-[44] and foreign scientists have conducted a series of mechanical tests under various stress states using modern SHPB testing machines, digital photography, acoustic emission, computed tomography, and other testing equipment, focusing on the anisotropic mechanical behaviour of complex-structured crystalline mass. They conducted a large series of studies on the macro- and micro-mechanical properties, energy dissipation characteristics, and the mechanisms of fracture development of stratified (cracked) crystalline rock mass. Convincing research results have been obtained. For example, Aliabadian et al., and Zhao et al. [45], [46] used the Digital Image Correlation (DIC) method to study the initiation, propagation, and penetration of cracks in stratified sandstone using the Brazilian splitting test method. Li et al. [47] conducted dynamic and static tests on the adhesion of stratified coal rocks and used computed tomography to characterize the internal morphology of coal rock cracks with different β values. Sun et al. [48] conducted Type I fracture tests on NSCB coal samples with different sizes and β angles, using an improved semicircular bending test, and studied the effect of sample size and β value on fracture viscosity and fracture mode of coal seam. Wang et al. [49] investigated the uniaxial compressive strength of a stratified crystalline rock mass at various strength ratios and revealed a correlation between the difference in strength of the lithological unit, the percentage soft rock content, and the uniaxial compressive strength of alternating stratified crystalline mass of soft and hard rocks. Wen et al. [50] used an SHPB testing device to conduct splitting tests on composite rocks with different values of β angles using the dynamic Brazilian method, and also studied the crack growth mode of samples in conjunction with high-speed digital camera system recording. Gao et al. [9][9] developed an elastic-plastic model with mixed initial and stress-induced anisotropy for a cracked (stratified) crystalline mass and, in combination with the strength criterion of crystalline material and the plane of layers, derived an anisotropic fracture formula for a cracked crystalline mass. Huang et al. [51], [52] obtained a new anisotropic viscoelastic-plastic model that can describe the three-stage anisotropic characteristics of a cracked (stratified) crystalline mass creeping, and then, the Mohr-Coulomb and Hoek-Brown criteria were derived. Two transverse isotropic strength criteria based on Jäger's weak plane theory and maximum axial strain were determined. Xia et al. [53] developed a microscopic damage criterion applicable to a cracked (stratified) complex-structured crystalline mass within the framework of the Non-local Macro-Meso-scale Damage (NMMD) theory.

In practical design and construction of engineering objects, the mechanical characteristics of rocks and the laws of origin and propagation of micro-cracks form the basis for assessing the stability of stratified crystalline rock mass. 3D-visualization of the distribution, propagation and evolution characteristics of micro-cracks has always been a focus of research in rock mechanics. The most commonly used method is numerical calculation, but the evolution of crack growth obtained by numerical calculation is difficult to reconcile with the actual growth of rock cracks under load conditions.

To reveal the characteristics of micro-cracks in a stratified crystalline mass, scanning electron microscopy, acoustic emission and computed tomography were used in mechanical tests to study the anisotropic behaviour of a complex-structured crystalline mass [54], [55]. However, existing studies typically describe the morphology of micro-cracks in accordance with the morphology of macro- and micro-cracks after fracture and do not provide an accurate description and quantitative analysis of the evolution of micro-cracks. The process of rock fracture is in fact a phenomenon of instability caused by the energy applied during the loading process. Deformation and fracture of rocks are closely related to the transformation of their energy, and the laws of energy evolution can more accurately reflect the nature of deformation and fracture of rocks [56], [57].

In connection with the above, conduct of true triaxial experimental and theoretical studies in brittle-plastic area, in which a cracked complex-structured crystalline mass is examined as a research object, based on the mechanism of energy dissipation and the fracture modes of stratified crystalline masses at various values of crack development angles (bedding), applied load and 3D-imaging of micro-crack development inside a sample throughout its height, is a relevant scientific and applied task. The research results may contribute to the further development of the theory basics and methods of mechanics of cracked (stratified) crystalline mass fracture, disaster prediction during mining operations at mining enterprises.

2. Materials and methods

2.1. Selection and preparation of samples for testing

To conduct tests under triaxial stress state of a cracked complex-structured crystalline mass and to assess the influence of physical-mechanical properties and its structural peculiarities on the change in the fracture nature, experimental studies were carried out in laboratory and in-situ conditions.

The main stages of preparing a complex-structured crystalline mass for testing are as follows. Rock samples (lumps) for testing were collected outside the zone of influence of technological processes of mineral mining in the preparatory workings of the Central SE VOSTGOK uranium mine, main line of the subway under construction (Dnipro), and on the benches of Ukrainian granite quarries – Sivach, Novopavlovsky, and Kapustiansky – for mining construction raw materials. The rocks in these masses are located in a tectonic-metasomatic zone with faults in the form of a monolithic crystalline granite mass of complex structure, medium cracking, and a strength of 12-18 to 20 points.

From selected lumps close to a cube shape with a linear size of ≈350 mm, models were produced in laboratory conditions by cutting the lumps on a stone-cutting machine with a 450 mm diameter diamond disc. For tests to determine the physical-mechanical properties, the samples were shaped into cubes with a rib size of 40 ± 2 mm, and the influence of triaxial stress state was tested on a cracked complex-structured crystalline mass with a rib size of 100×100×100 mm. Fifteen models were prepared for tests (three models for each type of rock). The faces of the samples were treated with grinding powder, with their curvature not exceeding 0.05 mm. The end surfaces (faces) of the samples were controlled using a gauge (caliper) along two mutually perpendicular faces. The deviation of the faces from parallelism was no more than ±0.1 mm.

For a detailed analysis of test results on determining the physical-mechanical properties of complex-structured crystalline rock mass and calculating its main characteristics, such as density, uniaxial compressive strength, longitudinal and transverse wave velocity, Poisson's ratio, and Young's modulus, test methods were used in accordance with current government standards [58]-[61]. The main parameters of the acoustic and physical-mechanical characteristics of the studied rock samples are given in Table 1. To confirm the adequacy of the obtained experimental results for the prepared complex-structured crystalline mass for real geological conditions, the results of uniaxial compression tests of the prepared samples were compared with each other. It was found that their uniaxial compressive strength and the fracture mode of the crystalline mass are similar. The obtained test data confirm the good consistency of the proposed method results.

Table 1. Physical-mechanical properties of rocks

No.	Rock type	Density, ($\rho \cdot 10^{-3}$), kg/m^3	Ultimate strength		Longitudinal wave velocity (V_p), m/s	Poisson's ratio, ν	Young's modulus (E), GPa
			in uniaxial compression (σ_{compr}), MPa	in uniaxial tension (σ_{tens}), MPa			
1	Pink coarse-grained granite	2.80	180.0	5.6	4350	0.22	19.2
2	Red coarse-grained granite	2.55	210.6	6.5	5100	0.28	16.6
3	Pegmatoid granites	2.60	150.0	4.6	6300	0.25	17.6
4	Albitite on granites	2.98	255.0	8.0	6380	0.23	13.0
5	Coarse-grained granite	2.61	138.8	4.3	6400	0.36	16.3

2.2. Scheme of the experiment

To test triaxial compression of cracked complex-structured crystalline masses, a mechanical system for loading samples of non-uniform component (multi-gradient) triaxial compression was used: a bench for self-sustaining fracture of rock samples, developed at the M.S. Poliakov Institute of Geotechnical Mechanics (IGTM) of the National Academy of Sciences of Ukraine.

The test bench layout is shown in Figure 1. It consists of a closed working chamber (Fig. 2a), the volume of which changes in accordance with the change in the sample volume (Fig. 2b), the ability to create in three mutually perpendicular directions (coordinates x_i, y_i, z_i) of a loaded system – hydraulic cylinders – independent stresses similar in value and direction to rock mass stresses with simultaneous fixation of strains by displacement strain gauges.

The test object in this research was coarse-grained red granite, which is an exclusively collective type of rock in a complex-structured crystalline mass, for example, in the conditions of driving the mine workings at the Central Mine (SE VOSTGOK), main line of the subway under construction (Dnipro, Ukraine) and granite masses in quarries for mining construction raw materials (Ukraine).

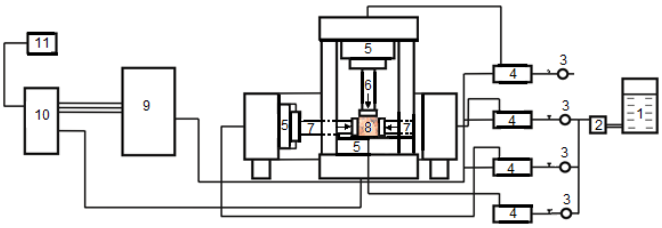

Figure 1. Test bench layout: 1 – container with working agent – industrial oil; 2 – pressure pump; 3 – pressure gauges; 4 – pressure reducing valves; 5 – support plates of the bench; 6, 7 – hydraulic loading rod vertical and horizontal, respectively; 8 – granite sample; 9 – bench control panel; 10 – data logger; 11 – computer

(a) (b)

Figure 2. Exterior view of the working chamber (a) for loading samples and a granite sample (b)

At the construction sites of underground structures (mine workings, tunnels), several fault zones were uncovered in the direction of their driving, according to geological survey data, where the crack planes in the fault zones show various dip angles ranging from 70 to 90°. Rock types in the fault zones correspond to the rocks near the mine working contours, and the cracks in the crystalline mass are filled (healed) with quartz aggregates within their boundaries (Fig. 3).

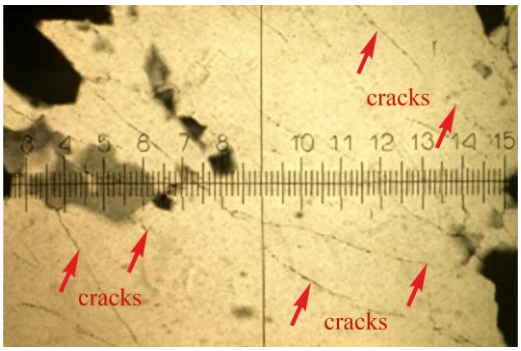

Figure 3. Microphotograph of an oriented petrographic thin section of coarse-grained red granite with cracks in mineral grains

The granite selected for testing has a homogeneous mineral composition with medium cracking. The uniaxial compressive strength (σ_{compr}) and uniaxial tensile strength (σ_{tens}) of rock samples were 210.6 and 6.5 MPa, respectively (Table 1). The crack geometry in natural crystalline rock mass is complex, and crack opening, roughness and direction have a significant influence on the nature of fracture.

During triaxial compression testing of crystalline mass samples, several types of crack inclination angles were identified depending on bedding, namely $\beta = 0$, 15, 45, 75, 90°. In accordance with the actual rock mass SSS conditions in mine workings during sample testing, four types of limiting pressures were assumed, namely $\sigma_3 = 5$, 10, 15 and 20 MPa. In this case, the average principal stress value can be represented by two extreme principal stress values, namely:

$$\sigma_2 = 0.5(\sigma_1 + \sigma_3) + \mu(\sigma_1 + \sigma_3). \quad (1)$$

Then the Noda-Lode index (coefficient) for principal stress strains can be represented as:

$$\mu = 2\left[\frac{(\sigma_2 - \sigma_3)}{(\sigma_1 - \sigma_3)}\right], \quad (2)$$

where:

$\sigma_1 \geq \sigma_2 \geq \sigma_3$;

σ_1 – vertical principal stress perpendicular to bedding (crack);

σ_2 and σ_3 – horizontal principal stresses parallel to bedding (crack).

The test procedure is as follows:

1. The prepared test sample is placed on the load platform of the working chamber and a preliminary load of 0.5 MPa is applied to the sample by moving the upper load plate and supplying a working agent (hydraulic oil) to the working system of the vertical hydraulic cylinder, followed by fixing it on the test sample face surface.

2. On the working surface of the bench pump unit, through the hydraulic system for supplying the working agent (industrial oil) and for regulating the oil pressure in the system, DR20 5 50 Y type pressure reducing valves are used, with which the working pressure in the system for testing is set independently for each hydraulic cylinder (vertical and horizontal) according to the pressure control device (manometer) readings, equal to 40 MPa. After preparing the system for testing with the application to the sample of the corresponding values of the limiting all-round pressure on all axes at a level of 5 MPa/min, loading is performed at a loading rate of 0.005 mm/s until the sample is fractured.

3. Simultaneously with conducting triaxial compression tests on samples, our research used a microscopic method to assess crack formation and their composition [62] using a modern GAOSUO P digital scanning microscope with 600-1200X digital zoom (manufactured by GAOSUO), equipped with a built-in 4.3 or 7-inch TFT-display that can be rotated 90° relative to the studied surface of the tested sample, a high-resolution video camera (12 Mpx) with a 32 GB SD memory card (Fig. 4a). The peculiarity of this microscope is its ability to automatically capture video and record the process of sample fracture at the macro level. During testing, the microscope on a stand was attached to the test bench base in the direction of fixed (clamped) test bench chamber plate with a pass-through window simulating the mine working contour, followed by scanning of the sample faces under triaxial loading.

4. To assess the characteristics of micro-cracks in a stratified (cracked) crystalline mass in mechanical tests with varying SSS parameters in rock samples, an effective method of real-time rock fracture monitoring – acoustic emission (AE) method – was used. The exterior view of the device for measuring the amplitude and frequency of AE propagation (manufacturer: DiSP Physical Acoustics Corporation, USA) is shown in Figure 4b.

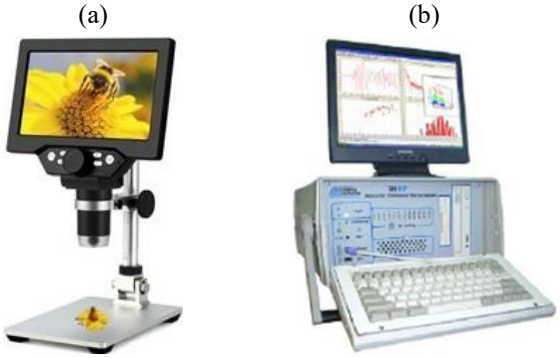

Figure 4. Instruments used in the research: (a) GAOSUO P digital scanning microscope – 600-1200 X; (b) device for measuring the amplitude and frequency of AE propagation

In this research, triaxial compressive stresses were tested on samples of five granite types (Table 1) using a test bench developed at the IGTEM NAS of Ukraine (Fig. 1). For the tests, the minimum principal stress values (σ_3) were determined, namely 5, 10, 15, 20 MPa, and the intermediate principal stress (σ_2) varied from one test cycle to another at the same σ_3 value. AE signals, their frequency and amplitude were recorded using six NANO-type resonant narrow-band sensors with a response frequency of 125 (750) kHz and 2/4/6 preamplifiers. Six AE sensors were uniformly fixed on six load plates: three rigid and three movable in six directions around the sample with Di sensor coordinates equal to (x_i, y_i, z_i) (i = 1, 2, 3, 4, 5, 6 – sensor numbers). Without pre-

liminary wave velocity measurement [63], a localization method was used during the experiments to obtain the true location of AE signal emissions. The results of recording the AE signals and their control in granite samples were processed using AE-win software.

In this research, it was assumed that for sensors with coordinates (x_i, y_i, z_i), the signal transmission start time is t_0, and the arrival of the P-wave at sensor Di is t_i (i = 1, 2, 3, 4, 5, 6), under the following condition:

$$(x_i - x)^2 + (y_i - y)^2 + (z_i - z)^2 = v^2 (t_i - t_0)^2, \quad (3)$$

where:

v – an indicator of the unknown P-wave velocity along the path of propagation.

Furthermore, when at least four sensors are activated, Equation (3) can be used to determine the coordinate of the radiation source, that is, (x, y, z) inside the sample space, by filtering the acceptable value of the AE signal.

The following setup tests were performed prior to experiment. Thus, σ_1 was applied along the z-direction, σ_2 – along the y-direction, and σ_3 – along the x-direction, respectively. The load control mode was set to a loading rate of 0.3 MPa/s. The procedure for conducting setup tests is as follows:

– to hold the rock sample in the chamber in its initial position, an initial load of 1 MPa (σ_1, σ_2, σ_3) was applied in the direction of the x, y, z axes, and then these three loads (σ_1, σ_2, σ_3) were increased until σ_3 reached the pre-fracture value of the sample;

– loads σ_1 and σ_2 on samples along the y and z axes were increased until σ_2 reached its limit value, while σ_3 was kept constant;

– load values σ_1 were increased to values at which the rock sample is fractured, while loads σ_2 and σ_3 were kept constant.

After the sample is fractured, the axial load is stopped by removing the limiting pressure and the damaged sample is removed from the load chamber. After triaxial compression tests are completed, the fractured granite samples are examined using computed tomography methods to study the behaviour of an anisotropic complex-structured crystalline mass. To study the structure, nature of crack formation and changes in the properties of an anisotropic complex-structured crystalline mass, and to obtain high-resolution images of the fractured sample at the microscopic level, an industrial Micro-CT scanner from the manufacturer GE Healthcare was used.

2.3. Energy calculation method

In triaxial compression tests, the total energy of the stratified rock mass U_t includes: energy U_0 generated at the hydrostatic pressure stage, axial energy U_1 generated by the work of vertical stress during mechanical testing, and negative work U_3 performed by the all-round pressure on the sample. The calculation formula is as follows [64]:

$$(x_i - x)^2 + (y_i - y)^2 + (z_i - z)^2 = v^2 (t_i - t_0)^2; \quad (4)$$

$$U_t = U_1 + U_3 + U_0 = \int_0^{\varepsilon_1} \sigma d\varepsilon_1 + 2\int_0^{\varepsilon_3} \sigma_3 d\varepsilon_3 + U_0. \quad (5)$$

During mechanical testing, U_t is converted into elastic energy U_e, accumulated in the samples, which can be released, and dissipated energy U_d, consumed by the expansion of internal cracks and friction during the development of damage and rupture of the sample. Then the calculation formula can be represented as:

$$U_t = U_d + U_e; \quad (6)$$

$$U_e = \frac{1}{2E_v}\left[\sigma_1^2 + 2\sigma_3^2 - 2\mu\left(2\sigma_1\sigma_3 + \sigma_3^2\right)\right], \quad (7)$$

where:

μ – the Poisson's ratio;

E_v – modulus of elasticity under de-stressing.

From a microscopic perspective, the development of rock fracture process involves the initiation, expansion and, finally, the unification of internal micro-cracks into macroscopic cracks. To reflect the change in dissipative energy at peak strength in a triaxial compression test, the ratio of dissipated energy U_{dp} at peak strength to total energy U_{tp} is determined as the dissipation rate D, that is:

$$D = \frac{U_d^p}{U_t^p}. \quad (8)$$

2.4. Method for calculating crack opening under conditions of volumetric stress state of a crystalline rock mass

It was found [65], [66] that between crack opening and the stress state of the crack surfaces at stresses σ_1 and σ_2, additional sample strain is formed exclusively in the σ_3 direction, without creating additional stress in the rock sample (Fig. 5). Consequently, this research is conducted based on the approach proposed above.

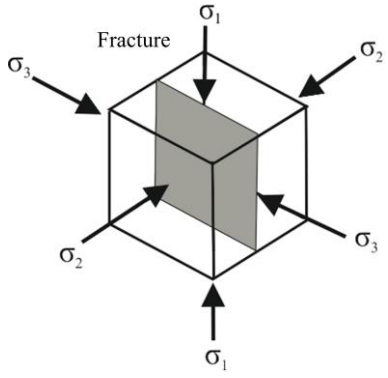

Figure 5. Schematic representation of triaxial stress state in a cracked crystalline rock mass

Suppose that when $\sigma_2 = \sigma_3$, the volumetric strain can be represented as:

$$\varepsilon_\upsilon = \varepsilon_1 + \varepsilon_2 + \varepsilon_3 = \frac{1-2\mu}{E}(\sigma_1 + \sigma_2). \quad (9)$$

Then the stress σ_1 and σ_2 applied in the direction σ_3 looks as follows:

$$\sigma_3 = \frac{E}{1+\mu}\left(\frac{\mu}{1-2\mu}\varepsilon_\upsilon + \varepsilon_3\right) = 0. \quad (10)$$

Then it is possible to schematically represent the stress curve and analyse it in a cracked crystalline rock mass under triaxial stress state (Fig. 6).

Thus, in the curve, σ_n and σ_x represent the normal stress and lateral stress on the crack surface, respectively. e – is the width of the crack opening in the horizontal direction.

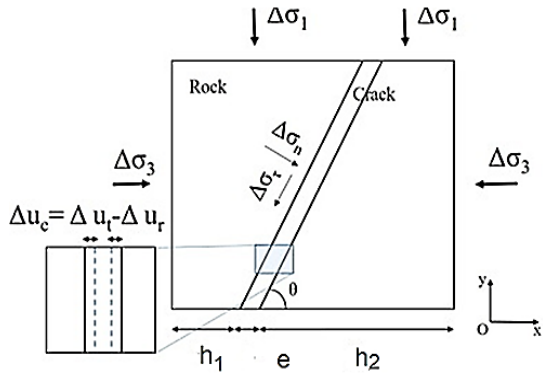

Figure 6. The nature of stress distribution in a cracked crystalline rock mass under triaxial stress state

h_1 and h_2 (Fig. 6) are the widths of the rock on either side of the crack. The analysis revealed the following assumptions:

– the rock mass strain and its fracture are subject to Hooke's general law;

– crystalline mass strain in the normal crack direction consists of rock skeleton strain (u_r) and crack strain (u_c). The total displacement (Δu_t) in the normal crack direction is equal to the sum of rock skeleton displacement (Δu_r) and crack displacement (Δu_c). In this case, compression is considered a positive action for tensile strain – a state of tensile stress and shear stress.

Given these assumptions, a new method for calculating crack strain can be proposed in this research. Normal crack strain can be determined as the difference between the total crystalline mass strain in the normal direction of the crack plane and the rock strain in the normal direction of the crack. Then the crack strain can be represented by the expression:

$$\Delta u_c = \Delta u_t - \Delta u_r = \frac{h_1 + h_2 + e}{sin\theta}\Delta\varepsilon_n - \frac{h_1 + h_2}{\sin\theta}\Delta\varepsilon_r, \quad (11)$$

where:

θ – is an angle between the crack and the horizontal direction of the applied load;

$\Delta\varepsilon_n$ – is the total crystalline mass strain at normal crack direction;

$\Delta\varepsilon_r$ – is rock skeleton strain at normal crack direction.

Then the normal and lateral stresses on the fracture plane can be expressed as:

$$\begin{cases} \sigma_n = \sigma_1 \cos\theta + \sigma_3 \sin\theta \\ \sigma_\tau = \sigma_1 \sin\theta - \sigma_3 \cos\theta \end{cases}. \quad (12)$$

Suppose that $\sigma_2 = \sigma_3$, then the increment in the cracked crystalline mass strain in the normal direction can be expressed as:

$$\Delta\varepsilon_3 = \frac{1}{E_{f+r}}\left[\Delta\sigma_n - \mu\left(\Delta\sigma_\tau + \Delta\sigma_3\right)\right], \quad (13)$$

where:

E_{f+r} – the modulus of elasticity of a cracked crystalline mass.

When rock skeleton layers shift in a direction normal to the crack, its strain can be expressed as:

$$\Delta\varepsilon_r = \frac{1}{E_r}\left[\Delta\sigma_n + \Delta P - \mu\left(\Delta\sigma_\tau + \Delta\sigma_3\right)\right], \quad (14)$$

where:

E_r – the rock skeleton elasticity modulus;

ΔP – the pressure difference between the inlet and outlet of fluid on the surface of the rock skeleton and crack under triaxial stress state.

Then, substituting Equations (12), (13), (14) into Equation (11), it is possible to obtain the total fracture strain:

$$\begin{cases} \Delta u_c = \chi\left[\Delta\sigma_n - \mu\left(\Delta\sigma_\tau - \Delta\sigma_3\right)\right] - \dfrac{h_1 + h_2}{E_r \sin\theta}\Delta P \\ \chi = \dfrac{h_1 + h_2 + e}{E_{f+r}\sin\theta} - \dfrac{h_1 + h_2}{E_r \sin\theta} \end{cases}. \quad (15)$$

Previous comprehensive studies conducted by Sun and Lin [67] showed an exponential correlation between the width of crack opening during its tension and rupture (shear) and normal strain. An equation was proposed to describe the variation relationship between normal strain under tensile stress and shear stress with crack opening width described by Expression (16):

$$e = e_0 \exp\left(-\lambda\frac{\sigma_n}{K_n}\right), \quad (16)$$

where:

e_0 – the initial crack opening width;

λ – a coefficient influencing the normal crack strain.

Then, according to the proposed method of this research, the ratio between normal stress and stiffness in the above equation can be simplified by replacing normal strain in the formula for calculating the crack opening width, namely:

$$e_n = e_{n0}\exp\left(-\lambda\varepsilon_n\right). \quad (17)$$

In this equation, ε_n characterizes the influence of lateral stress and normal stress on crack rupture (shear) strain:

$$\Delta\varepsilon_n = \frac{\Delta u_c}{e\sin\theta}. \quad (18)$$

It follows that by substituting Equations (15), (18) into Equation (17), we obtain the order for calculating normal strain for the crack opening width, taking into account the influence of the crack inclination angle based on elasticity theory [68], [69]:

$$\begin{cases} e = e_{no}\exp-\lambda\left(\dfrac{\left[\Delta\sigma_n - \mu\left(\Delta\sigma_\tau + \Delta\sigma_3\right)\right]}{e_{no}}\chi - \dfrac{h_1 + h_2}{E_{re_o}\sin\theta}\Delta P\right) \\ e_{no} = e_o \sin\theta \end{cases}. \quad (19)$$

3. Results and discussion

In the practice of studying mechanical characteristics of rocks, the laws of formation and expansion of micro-cracks form the basis for assessing the stability of cracked crystalline mass. 3D-visualization of the characteristics of micro-crack distribution, propagation and development has always been a focus of attention and a major challenge in rock mechanics research. The most commonly used method is numerical calculation, but the crack growth evolution obtained by numerical calculation is difficult to reconcile with the actual crack growth in rock under load.

Scanning electron microscopy, acoustic emission and computed tomography were used to identify the characteristics of micro-cracks in cracked rock mass during mechanical testing and to study the anisotropy of the cracked complex-structured rock mass [54], [55]. However, existing studies

generally describe the morphology of micro-cracks qualitatively, based on the morphology of macro- and micro-cracks after fracture, and do not contain a precise description and quantitative analysis of the evolution of micro-cracks. The process of rock fracture is in fact a phenomenon of energy instability. The strain and fracture of rocks are closely related to the conversion of their energy, and the laws of energy release can more accurately reflect the nature of rock strain and fracture [57][57], [58].

A cracked, complex-structured rock mass was selected as the object for testing of triaxial compression. Mechanical tests used methods to determine physical-mechanical properties, while the anisotropy of the cracked rock mass was studied using computer tomography methods with an industrial Micro-CT scanner from manufacturer GE Healthcare. Based on the energy release mechanism, the fracture mechanism of cracked mass samples at different crack inclination angles β and applied load σ_3 was analysed. "Stress-strain" dependences were constructed for tension of a cracked rock mass (Fig. 7).

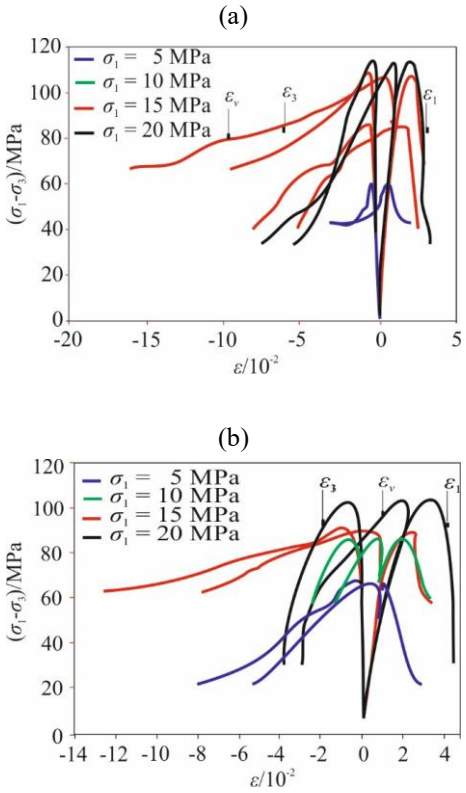

Figure 7. Typical "stress-strain" dependences for tension in a cracked rock mass with various crack inclination angles β and applied load σ_3: a – β = 0°; b – β = 15°

It was determined that in tests on a triaxial stress state, the value σ_3 has a significant influence on the characteristics of the "stress-strain" curve of a cracked rock mass.

At different values of β and σ_3, the compaction stage of the samples is relatively short, which is not obvious when compared to the overall process of change in the "stress-strain" curve. This means that the prepared samples are relatively dense, with few internal pores and initial cracks.

The value σ_3 has a significant influence on the strength and strain characteristics of samples with different values of β. Thus, with an increase in σ_3, σ_1-σ_3, ε_1, ε_3, ε_v and a corresponding increase in all-round pressure and strain, cracked rock samples become capable of resisting external loads and strains.

When σ_3 is small, the linear elastic component has a greater proportion in the "stress-strain" curve section than in the yield curve section as the σ_3 increases. The yield stage is a larger proportion, indicating that the higher the σ_3 value, the higher the plastic strain ability of the sample, and the slopes of the "stress-strain" curves at different β values also show obvious changes.

Based on the physical-mechanical properties of cracked samples of complex-structured crystalline rocks (Table 1), the influence of β and σ_3 on the peak stress (σ_{1p}) and peak differential stress (σ_{pd}) of the sample was studied, as presented in Figures 8 and 9, respectively.

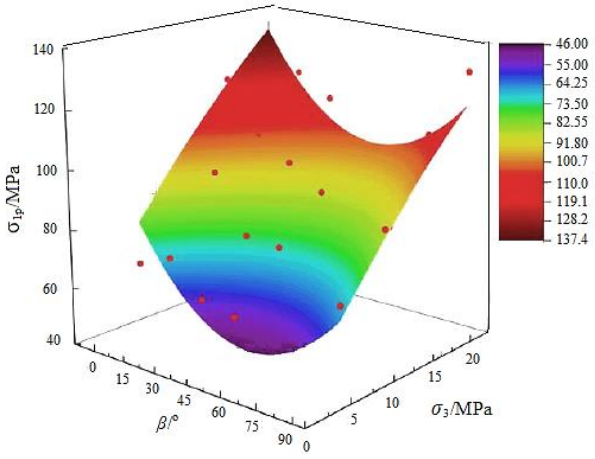

Figure 8. Peak stresses in cracked rock masses at various values of β and σ_3

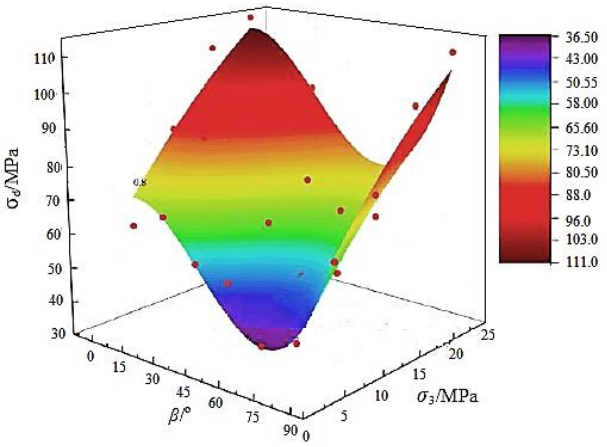

Figure 9. Peak differential stresses in cracked rock masses at various values of β and σ_3

With an increase in the value of σ_3, the values of σ_{1p} and σ_d increase almost linearly. That is, the resistance of samples to strain and fracture increases with increasing σ_3 value. The values of σ_{1p} and σ_d of the samples first decrease and then increase with increasing β. For different values of σ_3, the maximum values of σ_{1p} and σ_d are usually achieved at β = 0° or 90°, and the minimum values – at β = 60°. The ratio between the strength parameters σ_{1p} and σ_d, β and σ_3 are approximated by the regression equation and the coefficient of determination, namely:

$$\sigma_{1p} = 55.64 - 1.34 \cdot \beta + 5.07 \cdot \sigma_3 - 0.0015\beta \cdot \sigma_3 + \\ +0.0129 \cdot \beta^2 - 0.050 \cdot \sigma_3^2,\ R^2 = 0.9; \quad (20)$$

$$\sigma_d = 49.25 + 0.17 \cdot \beta + 4.07 \cdot \sigma_3 - 0.0015\beta \cdot \sigma_3 - \\ -0.029 \cdot \beta^2 - 0.050 \cdot \sigma_3^2 + 0.00031 \cdot \beta^2, R^2 = 0.95. \quad (21)$$

When analysing the "stress-strain" process, it becomes clear that the strain of triaxial compression of cracked granite can be divided into five stages.

Stage I – the compaction stage, characterized by strain in the cracked crystalline mass, which is essentially the same as in the undamaged rock mass.

Stage II – elastic strain stage shows a noticeable increase in the crack initiation stress σ_{ci} of the crystalline mass as the all-round pressure and crack angle increase.

Stage III – stage of steady expansion of cracks, stable expansion of composite cracks and the appearance of new cracks lead to a slower compression rate of volumetric crystalline mass strain. During this period, the degree of crack compression increases as the crack angle decreases, and the volumetric crack reduction becomes more evident at increased all-around pressure.

Stage IV – stage of rapid crack development, characterized by a significant increase in circumferential strain. When the fracture angle is 90 and 80°, the volumetric crystalline mass strain gradually changes from compression to expansion with increasing axial strain, but the degree of expansion decreases with increasing all-round pressure. On the contrary, when the fracture angle reaches 70°, the crystalline mass retains reduced volumetric strain, and this reduction becomes more significant with increasing all-around pressure.

Stage V – the post-peak fracture stage, during which the residual stress σ_{cr} increases with higher all-round pressure and fracture angle. In particular, when fracture angle is 90°, the residual strength approaches that of an intact crystalline rock mass.

To assess the characteristics of micro-cracks and macro-cracks in a cracked (stratified) crystalline mass in mechanical tests with varying SSS parameters in rock samples, an effective method of real-time rock fracture monitoring was used – the acoustic emission (AE) method. The exterior view of the equipment for measuring the amplitude and frequency of AE propagation is shown in Figure 4b. The test procedure is described in Section 2.

To identify AE signals (events) during testing, the occurrence and propagation of micro-cracks until they form macro-cracks, which subsequently contribute to rock fracture.

During testing, data were obtained on the count of AE signals and changes in stress state at various axial loads: 5, 10, 15, and 20 MPa. The obtained data were processed in Microsoft Excel environment and were used to construct dependences of changes in the temporal characteristics of the count of AE signals and compression stress at different axial loads. Figure 10 shows typical time characteristics of AE count and compression stress, for example, at an axial load of 5 MPa with an application rate of 1, 0.3, and 0.05 mm/min. Under various load disturbance conditions, three typical stages were recorded in the number of acoustic emission oscillations of a granite sample during triaxial compression: a quiet period, an eruption period, and post-peak release period. The quiet period corresponds to the compaction stage and the elastic stage of the loaded sample. In this case, when σ_1 varied from 50 to 93% of its peak value, the AE signal frequency and AE activation frequency values decreased significantly, and AE entered a quiet period, with a large dispersion in the distribution of the quiet period. The duration was 93-452 s, the average value was 239.79 s, and the dispersion was 114.81. The stress at the beginning of the quiet period was 27-91% of the maximum stress (average value – 69%).

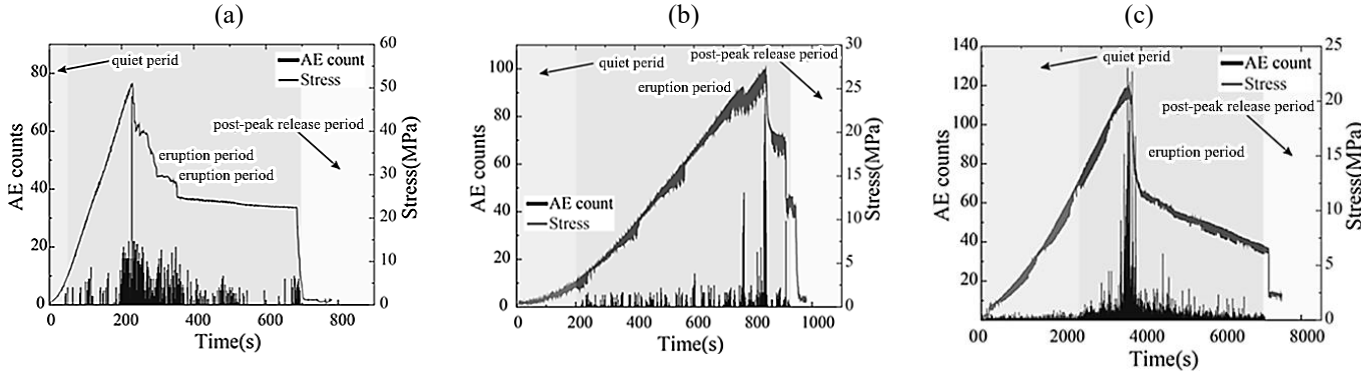

Figure 10. Time-varying characteristics of AE count and compressive stress under an axial load of 5 MPa at different loading rates: (a) 1 mm/min; (b) 0.3 mm/min; (c) 0.05 mm/min

During this period, the initial cracks inside the sample gradually close under the action of limiting pressure. Since the sample structure is relatively stable, the strain predominates due to the recoverable elastic strain, with a small total count of AE signals and their amplitude. The energy applied by the loaded triaxial compression system is mainly converted into elastic energy accumulation in the sample, and there is only a small amount of energy dissipation caused by crack friction, while the energy release effect is weak. The crack propagation stage and the stress drop stage of the loaded sample together constitute the crack rupture period. During this period, with a continuous increase in axial stress, new micro-cracks begin to appear inside the sample, facilitating further expansion and penetration of the initial cracks. The network of cracks gradually develops and ultimately forms a macroscopic crack surface that dominates during fracture. This process is accompanied by the generation of a large count of AE signals, which causes an explosive increase in the number of acoustic vibrations. In this case, the elastic energy accumulated in the sample is steadily released through crack propagation. When the sample reaches peak stress, the crack penetration rate is maximum, and the count of acoustic vibrations also reaches its maximum value. The post-peak release period corresponds to the residual strength stage after the stress drop in the granite sample. With the formation of a macroscopic fracture surface and a sharp

decrease in stress levels, the crack propagation activity inside the sample significantly weakens, and the acoustic emission signal demonstrates rapid attenuation or even disappears completely. This period represents a transitional process from peak strength to complete fracture, and its total duration is short.

When conducting tests for triaxial compression of samples in our research, we used a microscopic method to assess crack formation, width, depth, and composition [61] using a modern GAOSUO P digital scanning microscope with 600-1200× digital zoom (manufactured by GAOSUO), Figure 4a. Using these microscope characteristics during testing process, synchronous video recording was performed in automatic mode with rough and precise regulation, recording the process of sample fracture at the macro level with object magnification from 0 to 1200×. To do this, the microscope on a stand was attached to the bench base in the direction of fixed (clamped) bench chamber plate with a pass-through window simulating the mine working contour, followed by scanning the faces of the sample with an area of 10×10 cm under triaxial loading. Based on the results of scanning the fracture process of samples at the macro level, the results of sample fracture were obtained and all cracks were identified (Fig. 11). The characteristics of cracks after testing cracked crystalline mass samples are given in Table 2.

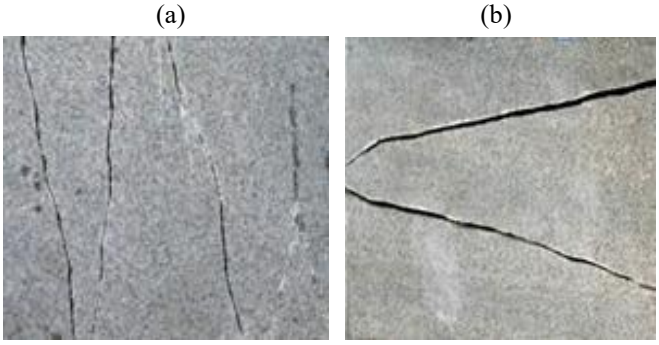

Figure 11. The nature of crack development after testing granite samples for triaxial compression: (a) medium-cracked granite; (b) slightly-cracked granite

Table 2. Results of microscopic analysis of rock samples after triaxial compression test

No.	Rock type	Sampling location	Density ($\rho \cdot 10^{-3}$), kg/m^3	Crack depth, μm	Crack width, μm	Number of cracks in the field of view of the microscope, pcs
1	Pink coarse-grained granite	PRJSC "Sivach" Quarry, Cherkasy Oblast	2.80	90	5-10	5
2	Red coarse-grained granite	Kapustiansky Quarry, Kirovohrad Oblast	2.55	70	10	2
3	Pegmatoid granites	Ingulskaya Mine, the city of Kropyvnytskyi	2.60	100	5-6	5-8
4	Albitite on granites	Ingulskaya Mine, the city of Kropyvnytskyi	2.98	150	8-10	3-5
5	Coarse-grained grey granite	Novopavlovskyi Quarry, Kirovohrad Oblast	2.61	80-90	8-10	5

To obtain CT-scanning results of the all-round pressure influence on the fracture modes of cracked crystalline masses, granite samples with a crack inclination angle $\beta = 45°$ were selected. After completing the triaxial compression tests, the axial load is stopped by removing the limiting pressure, and the damaged sample is removed from the load chamber for examination using CT-tomography methods to study the behaviour of the anisotropic complex-structured crystalline mass.

To study the structure, nature of crack formation and changes in the properties of an anisotropic complex-structured crystalline mass, and to obtain high-resolution images of the fractured sample at the microscopic level, an industrial Micro-CT scanner from the manufacturer GE Healthcare was used. The results of CT-scanning of the fractured granite samples were processed using Avizo software and were used to subsequently obtain a 3D-image reconstruction of the micro-cracks inside the fractured sample (Fig. 12).

The figure shows that there is a good correlation between the main crack after 3D-reconstruction and the macro-fracture modes of the samples. In addition to the main crack, secondary cracks inside the samples are also widespread, and both the main crack and the secondary cracks jointly influence on the change in the crack growth rate (v_{crack}). As σ_3 value increases, v_{crack} value first increases and then decreases. When σ_3 is 10 and 20 MPa, the v_{crack} value reaches its maximum and minimum values, respectively.

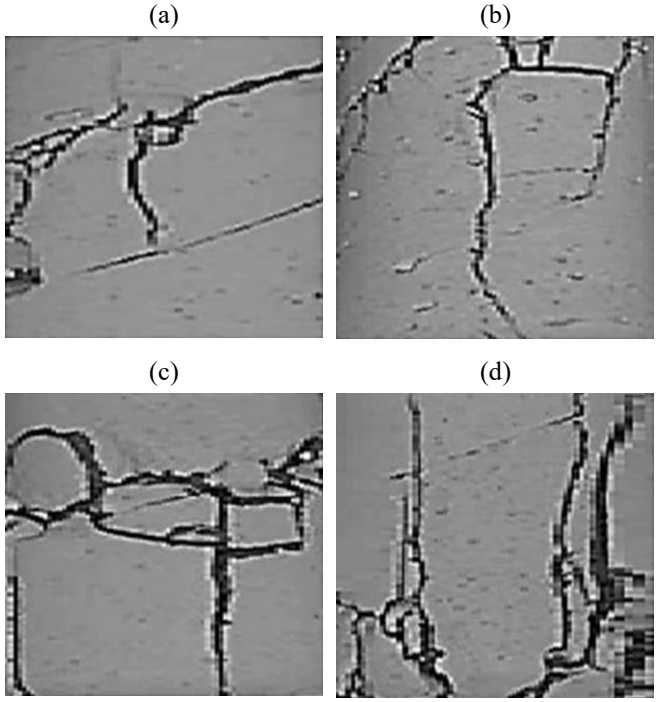

Figure 12. 3D-reconstruction of stratified rock samples based on computed tomography: (a) σ_3 = 5 MPa; (b) σ_3 = 10 MPa; (c) σ_3 = 15 MPa; (d) σ_3 = 20 MPa

4. Conclusions

This research is devoted to conducting true triaxial experimental and theoretical studies in the brittle-plastic area, in which a cracked complex-structured crystalline mass is examined as a research object. Based on the identified energy release mechanisms and fracture modes of stratified crystalline masses at different values of crack development angles (bedding) and applied load, 3D-images of micro-crack development throughout its height inside the sample were obtained.

The results show that as the limiting pressure increases, the ability of the sample to accumulate energy increases. The σ_3 value has a significant influence on the anisotropy coefficient and the fracture energy value at peak strength of the samples.

Under the influence of the crack (layer) inclination angle, the fracture modes of cracked crystalline rock samples exhibit three typical characteristics with increasing σ_3 value. The anisotropy coefficients of energy values at peak strength of rock samples vary greatly in their sensitivity to β value. The sensitivity of dissipative energy to β value is the highest, while the sensitivity of elastic energy to β value is the lowest.

The results of CT-scanning and 3D reconstruction of cracked (stratified) rock samples at a crack inclination angle of $\beta = 45°$ show that the reconstructed main crack corresponds well to the macro-modes of sample fracture. Due to the combined action of the main crack and secondary cracks, the crack growth rate first increases and then decreases as the σ_3 value increases.

The development of AE events during rock fracture has a clear three-stage structure: the initial quiet period is characterized by the predominance of elastic strain, with weak acoustic emission activity; during crack propagation period, a macroscopic crack forms with the primary crack penetration, and the acoustic emission parameters increase exponentially and reach an extreme value at peak stress. The attenuation period after the peak decreases rapidly as the stress reduces.

At constant limiting pressure, increasing the loading rate reduces the count of AE events, but significantly increases the value of peak energy release and exacerbates sample fracture. At the same loading rate, a decrease in the limiting pressure simultaneously increases the count of AE events and the intensity of energy release, which leads to an increase in the degree of the sample damage.

The research results can provide a theoretical basis for further development of the fracture mechanics of cracked (stratified) crystalline mass, disaster prediction during mining operations at mining enterprises.

Author contributions

Conceptualization: OI, RK, KI; Formal analysis: RK; Funding acquisition: OI, KI; Investigation: OI, LN, IP, VK, RK, KI; Methodology: LN, IP, RK; Project administration: KI; Resources: IP, VK; Software: OI, LN; Supervision: IP, VK, KI; Validation: VK; Visualization: OI, LN, VK; Writing – original draft: LN, IP; Writing – review & editing: OI, RK, KI. All authors have read and agreed to the published version of the manuscript.

Funding

Research was conducted according to complex program of the National Academy of Sciences of Ukraine on the nuclear energy development "Development of scientific bases and improvement of methods and means of increasing the efficiency and safety of mining operations in uranium ore mining" (No. GR 0117U004231) and the agreement on scientific-technical cooperation between M.S. Poliakov Institute of Geotechnical Mechanics of the National Academy of Sciences of Ukraine, Dnipro University of Technology, Cherkasy State Technological University and AGH University of Science and Technology.

Acknowledgements

We thank the colleagues from the National Academy of Sciences of Ukraine for their support. We also acknowledge the contributions of researchers from M.S. Poliakov Institute of Geotechnical Mechanics of the National Academy of Sciences of Ukraine, Dnipro, University of Technology, Cherkasy State Technological University and AGH University of Science and Technology, Poland.

Conflicts of interests

The authors declare no conflict of interest.

Data availability statement

The original contributions presented in the study are included in the article, further inquiries can be directed to the corresponding author.

References

[1] Chen, Z., He, C., Xu, G., Ma, G., & Yang W. (2019). Support mechanism and mechanical behavior of double primary support method for tunnels in collapsed phyllite under high geostress conditions: A case study. *Bulletin of Engineering Geology and the Environment*, *78*(7), 5253-5267. https://doi.org/10.1007/s10064-019-01479-1

[2] Cheng, Q., Xiao, S., Liu, T., Chen, T., Li, S., & Wei, A. (2021). Twin tunneling-induced deep-seated landslide in layered sedimentary rocks. *Bulletin of Engineering Geology and the Environment*, *80*(12), 9071-9088. https://doi.org/10.1007/s10064-021-02482-1

[3] Man, J., Zhou, M., Zhang, D., Huang, H., Chen, J. (2022). Face stability analysis of circular tunnels in layered rock masses using the upper bound theorem. *Journal of Rock Mechanics and Geotechnical Engineering*, *14*(6),1836-1848. https://doi.org/10.1016/j.jrmge.2021.12.023

[4] Tan, X., Ren, Y., Li, T., Zhou, S., Zhang, J., & Zhou, S. (2021) In-situ direct shear test and numerical modeling of structural planes of shale with thick silty intermediate layer along the bedding slope. *International Journal of Rock Mechanics and Mining Sciences*, *143*, 104791, 143. https://doi.org/10.1016/j.ijrmms.2021.104791

[5] Sun, X., Pang, S., Qin, K., Shi, T., Zhu, C., & Tao, Z. (2022). Analysis of blasting vibration signal of high steep anti-dip layered rock slope. *Journal of Mountain Science*, *19*, 3257-3269. https://doi.org/10.1007/s11629-022-7414-6

[6] Chen, J., Liu, W., Chen, L., Luo, Y., Li, Y., Gao, H., & Zhong, D. (2020). Failure mechanisms and modes of tunnels in monoclinic and soft-hard interbedded rocks: A case study. *KSCE Journal of Civil Engineering*, *24*(4), 1357-1373. https://doi.org/10.1007/s12205-020-1324-3

[7] Krukovskyi, O.P., Kurnosov, S.A., Makeyev, S.Y., & Stadnychuk, M.M. (2023). Determination of the reliability of mine support equipment considering its deformation risks. *Strength of Materials*, *55*(3), 475-483. https://doi.org/10.1007/s11223-023-00540-5

[8] Suo, Y., Chen, Z., Rahman, S., &Song, H. (2020). Experimental and numerical investigation of the effect of bedding layer orientation on fracture toughness of shale rocks. *Rock Mechanics and Rock Engineering*, *53*, 3625-3635. https://doi.org/10.1007/s00603-020-02131-1

[9] Gao, M., Gong, B., Liang, Z., Jia, S., & Zou, J. (2023). Investigation of the anisotropic mechanical response of layered shales. *Energy Science & Engineering*, *11*(12), 4737-4754. https://doi.org/10.1002/ese3.1611

[10] Lisjak, A, Grasselli, G, & Vietor, T. (2014). Continuum-discontinuum analysis of failure mechanisms around unsupported circular excavations in anisotropic clay shales. *International Journal of Rock Mechanics and Mining Sciences*, *65*, 96-115. https://doi.org/10.1016/j.ijrmms.2013.10.006

[11] Han, Z., Qiao, C., & Xu, H. (2017). Analysis of strength anisotropy of rock mass with a set of persistent joints. *Journal of China University of Mining & Technology*, *46*(5), 1073-1083.
[12] Yang, Z., Gao, Y., & Wu, S. (2018). Study of the influence of joint parameters on rock mass strength based on equivalent rock mass technology. *Journal of China University of Mining & Technology*, *47*(5), 979-986.
[13] Cheng, J., Yang, S., & Yin, P. (2018). Experimental study of the deformation and strength behavior of composite rock specimens in unloading confining pressure test. *Journal of China University of Mining & Technology*, *47*(6), 1233-1242.
[14] Xie, H., Ju, Y., Gao, F., Gao, M., & Zhang, R. (2017). Groundbreaking theoretical and technical conceptualization of fluidized mining of deep underground solid mineral resources. *Tunnelling and Underground Space Technology*, *67*, 68-70. https://doi.org/10.1016/j.tust.2017.04.021
[15] Wang, H., Wang, Z., Wang, J., Wang, S., Wang, H., Yin, Y., & Li, F. (2021). Effect of confining pressure on damage accumulation of rock under repeated blast loading. *International Journal of Impact Engineering*, *156*, 103961. https://doi.org/10.1016/j.ijimpeng.2021.103961
[16] Ni, Y., Wang, Z., Li, S., Wang, J., & Feng, C. (2024). Numerical study on the dynamic fragmentation of rock under cyclic blasting and different in-situ stresses. *Computers and Geotechnics*, *172*, 106404. https://doi.org/10.1016/j.compgeo.2024.106404
[17] Wong, T., & Baud, P. (2012). The brittle-ductile transition in porous rock: A review. *Journal of Structural Geology*, *44*, 25-53. https://doi.org/10.1016/j.jsg.2012.07.010
[18] Liu, J., Jia, W., Duan, H., Li, X., & Xia, K. (2024). Experimental study on the deformation and failure characteristics of cement stone under true triaxial stress state. *Construction and Building Materials*, *449*, 138397. https://doi.org/10.1016/j.conbuildmat.2024.138397
[19] Xu, Y., Xiao, J., Liu, J., & Xia, K. (2024). True-triaxial strength characteristics of cement stone subjected to sulfuric acid corrosion: An experimental and theoretical study. *Construction and Building Materials*, *444*, 137877. https://doi.org/10.1016/j.conbuildmat.2024.137877
[20] Liu, J., Li, X., Xiao, J., Xie, Y., & Xia, K. (2024). Three-dimensional strength criterion for rocks: A review. *Energy Reviews*, *3*(4), 100102. https://doi.org/10.1016/j.enrev.2024.100102
[21] Vachaparampil, A., & Ghassemi, A. (2017). Failure characteristics of three shales under true-triaxial compression. *International Journal of Rock Mechanics and Mining Sciences*, *100*, 151-159. https://doi.org/10.1016/j.ijrmms.2017.10.018
[22] Chen, Z., Huang, L., Yan, L., Li, S., Cai, H., Li, Y., & Luo, X. (2024). Characterising mechanical properties and failure criteria of steel slag aggregate concrete under multiaxial stress states. *Construction and Building Materials*, *424*, 135903. https://doi.org/10.1016/j.conbuildmat.2024.135903
[23] Lu, D., Du, X., Wang, G., Zhou, A., & Li, A. (2016). A three-dimensional elastoplastic constitutive model for concrete. *Computers & Structures*, *163*, 41-55. https://doi.org/10.1016/j.compstruc.2015.10.003
[24] Cao, Z., Liu, J., Xiao, J., Zhang, J., & Xu, Y. (2024). Strength characteristics and energy evolution of cement stone under true-triaxial loading conditions. *Construction and Building Materials*, *432*, 136690. https://doi.org/10.1016/j.conbuildmat.2024.136690
[25] Feng, C., Wang, Z., Wang, J., Fu, J., & Lu, Z. (2024). The mechanism of low strain rate and moderate principal stress effects in triaxial prestressed marble under lateral impulsive load. *Soil Dynamics and Earthquake Engineering*, *184*, 108860. https://doi.org/10.1016/j.soildyn.2024.108860
[26] Liu, J., Li, X., Wang, C., Xu, Y., & Xia, K. (2024). A three-dimensional elastoplastic constitutive model incorporating Lode angle dependence. *Geomechanics for Energy and the Environment*, *38*, 100567. https://doi.org/10.1016/j.gete.2024.100567
[27] Song, Z., Zhang, Z., Ranjith, P. G., Zhao, W., & Liu, C. (2022). Experimental study on the influence of hydrostatic stress on the Lode angle effect of porous rock. *International Journal of Mining Science and Technology*, *32*(4), 727-735. https://doi.org/10.1016/j.ijmst.2022.02.007
[28] Jiang, H. (2017). A failure criterion for rocks and concrete based on the Hoek-Brown criterion. *International Journal of Rock Mechanics and Mining Sciences*, *95*, 62-72. https://doi.org/10.1016/j.ijrmms.2017.04.003
[29] Wu, S., Zhang, S., & Zhang, G. (2018). Three-dimensional strength estimation of intact rocks using a modified Hoek-Brown criterion based on a new deviatoric function. *International Journal of Rock Mechanics and Mining Sciences*, *107*, 181-190. https://doi.org/10.1016/j.ijrmms.2018.04.050
[30] Ma, X., Rudnicki, J.W., & Haimson, B.C. (2017). The application of a Matsuoka-Nakai-Lade-Duncan failure criterion to two porous sandstones. *International Journal of Rock Mechanics and Mining Sciences*, *92*, 9-18. https://doi.org/10.1016/j.ijrmms.2016.12.004
[31] Rudnicki, J.W. (2017). A three invariant model of failure in true triaxial tests on Castlegate sandstone. *International Journal of Rock Mechanics and Mining Sciences*, *97*, 46-51. https://doi.org/10.1016/j.ijrmms.2017.06.007
[32] Chemenda, A.I., & Mas, D. (2016). Dependence of rock properties on the Lode angle: Experimental data, constitutive model, and bifurcation analysis. *Journal of the Mechanics and Physics of Solids*, *96*, 477-496. https://doi.org/10.1016/j.jmps.2016.08.004
[33] Lee, Y.-K., Pietruszczak, S., & Choi, B.-H. (2012). Failure criteria for rocks based on smooth approximations to Mohr-Coulomb and Hoek-Brown failure functions. *International Journal of Rock Mechanics and Mining Sciences*, *56*, 146-160. https://doi.org/10.1016/j.ijrmms.2012.07.032
[34] Jiang, H. (2018). Simple three-dimensional Mohr-Coulomb criteria for intact rocks. *International Journal of Rock Mechanics and Mining Sciences*, *105*, 145-159. https://doi.org/10.1016/j.ijrmms.2018.01.036
[35] Shin, H., & Kim, J.-B. (2015). Physical interpretations for cap parameters of the modified Drucker-Prager cap model in relation to the deviator stress curve of a particulate compact in conventional triaxial testing. *Powder Technology*, *280*, 94-102. https://doi.org/10.1016/j.powtec.2015.04.023
[36] Vicente da Silva, M., & Antão, A.N. (2023). A new Hoek-Brown-Matsuoka-Nakai failure criterion for rocks. *International Journal of Rock Mechanics and Mining Sciences*, *172*, 105602. https://doi.org/10.1016/j.ijrmms.2023.105602
[37] Xie, H., Gao, M., Zhang, R., Peng, G., Wang, W., & Li, A. (2018). Study on the mechanical properties and mechanical response of coal mining at 1000 m or deeper. *Rock Mechanics and Rock Engineering*, *52*(5), 1475-1490. https://doi.org/10.1007/s00603-018-1509-y
[38] Feng, C., Wang, Z., Wang, J., Lu, Z., & Li, S. (2024). A thermo-mechanical damage constitutive model for deep rock considering brittleness-ductility transition characteristics. *Journal of Central South University*, *31*(7), 2379-2392. https://doi.org/10.1007/s11771-024-5700-x
[39] Li, M., Lu, J., Xie, H., Gao, M., Gao, H., Shang, D., & Jiang, C. (2024). Nonlinear mechanical and 3D rupture morphology of saturated porous sandstone under true triaxial stress. *Rock Mechanics and Rock Engineering*, *57*(9), 6837-6859. https://doi.org/10.1007/s00603-024-03884-9
[40] Aleksieiev, A.D., Revva, V.N., & Riazantsev, N.A. (1989). *Fracture of rocks in volumetric compression stress field*. Kyiv, Ukraine: Naukova dumka, 168 p.
[41] Vasiliev, L.M., Vasiliev, D.L., & Malich, N.G. (2021). *Self-organization of forms of destruction of rock samples during their compression*, London, United Kingdom: Lap Lambert Academic Publishing, 243 p.
[42] Vasiliev, L.M., Vasiliev, D.L., Malich, M.G., & Anhelovskyi, O.O. (2017). Analytical method for calculating and charting "stress-deformation" provided longitudinal form of destruction of rock samples. *Naukovyi Visnyk Natsionalnoho Hirnychoho Universytetu*, *3*, 74-80.
[43] Vasyliev, L.M., Vasyliev, D.L., Nazarov, O.E., Malich, M.G., & Katan, V.O. (2021). The method for determining the parameters of the diagrams of a truncated-wedge destruction of cylindrical samples of rocks. *Naukovyi Visnyk Natsionalnoho Hirnychoho Universytetu*, *1*, 47-52. https://doi.org/10.33271/nvngu/2021-1/047
[44] Vasyliev, L., Malich, M., Vasyliev, D., Katan, V., & Rizo, Z. (2023). Improving a technique to calculate strength of cylindrical rock samples in terms of uniaxial compression. *Mining of Mineral Deposits*, *17*(1), 43-50. https://doi.org/10.33271/mining17.01.043
[45] Aliabadian, Z., Zhao, G. F., & Russell, A. R. (2019). Crack development in transversely isotropic sandstone disks subjected to Brazilian testing observed using digital image correlation. *International Journal of Rock Mechanics and Mining Sciences*, *119*, 211-221. https://doi.org/10.1016/j.ijrmms.2019.04.004
[46] Aliabadian, Z., Zhao, G.F., & Russell, A.R. (2019). Failure, crack initiation and tensile strength of transversely isotropic rock using the Brazilian test. *International Journal of Rock Mechanics and Mining Sciences*, *122*, 104073. https://doi.org/10.1016/j.ijrmms.2019.104073
[47] Li, J., Zhao, J., Gong, S.Y., Wang, H.C., Ju, M.H., Du, K., & Zhang, Q.B. (2021). Mechanical anisotropy of coal under coupled biaxial static and dynamic loads. *International Journal of Rock Mechanics and Mining Sciences*, *143*, 104807. https://doi.org/10.1016/j.ijrmms.2021.104807
[48] Sun, Z., Zhao, Y., Gao, Y., Gao, S., Elmo, D., & Wei, X. (2024). Effect of size and anisotropy on mode I fracture toughness of coal. *Theoretical and Applied Fracture Mechanics*, *129*, 104170. https://doi.org/10.1016/j.tafmec.2023.104170
[49] Wang, Z., Wang, M., Zhou, L., Zhu, Z., Shu, Y., & Peng, T. (2022). Research on uniaxial compression strength and failure properties of stratified rock mass. *Theoretical and Applied Fracture Mechanics*, *121*, 103499. https://doi.org/10.1016/j.tafmec.2022.103499
[50] Wen, S., Huang, R., Zhang, C., & Zhao, X. (2023). Mechanical behavior and failure mechanism of composite layered rocks under dynamic tensile loading. *International Journal of Rock Mechanics and Mining Sciences*, *170*, 105533. https://doi.org/10.1016/j.ijrmms.2023.105533

[51] Huang, S., Zhang, J., Ding, X., Han, G., Yu, P., & Fan, X. (2024). A three-dimensional anisotropic creep model for predicting the time-dependent deformation of layered rock mass. *Rock Mechanics and Rock Engineering*, *57*(5), 3577-3600. https://doi.org/10.1007/s00603-023-03745-x

[52] Huang, S., Zhang, J., Ding, X., Zhang, C., Han, G., Yu, G., & Qu, L. (2024). Investigation of anisotropic strength criteria for layered rock mass. *Journal of Rock Mechanics and Geotechnical Engineering*, *16*(4), 1289-1304. https://doi.org/10.1016/j.jrmge.2023.06.006

[53] Xia, X., Wang, X., Lu, G., Gu, X., Lv, W., Zhang, Q., & Ma, L. (2024). A new nonlocal macro-micro-scale consistent damage model for layered rock mass. *Theoretical and Applied Fracture Mechanics*, *133*, 104540. https://doi.org/10.1016/j.tafmec.2024.104540

[54] Wang, S., He, C., Xu, G., Bai, R., Shu, Y., Wang, J., Yue, J., & Zhang, W. (2024). Investigating failure modes and Micro-Crack classification in Mao phyllite under notched Semi-Circular bend testing. *Theoretical and Applied Fracture Mechanics*, *130*, 104319. https://doi.org/10.1016/j.tafmec.2024.104319

[55] Liu, K., Zou, L., Guo, T., Guo, C., Yang, J., & Zhang, Y. (2024). Fracture behavior and acoustic emission characteristics of layered sandstone with a bedding-parallel crack. *Theoretical and Applied Fracture Mechanics*, *131*, 104344. https://doi.org/10.1016/j.tafmec.2024.104344

[56] Zhang, J., Du, R., Chen, Y., & Huang, Z. (2023). Experimental investigation of the mechanical properties and energy evolution of layered phyllite under uniaxial multilevel cyclic loading. *Rock Mechanics and Rock Engineering*, *56*(6), 4153-4168. https://doi.org/10.1007/s00603-023-03279-2

[57] Gao, M., Liang, Z., Jia, S., Zhang, Q., & Zou, J. (2023). Energy evolution analysis and related failure criterion for layered rocks. *Bulletin of Engineering Geology and the Environment*, *82*(12), 439. https://doi.org/10.1007/s10064-023-03445-4

[58] State Standard 21153.0-75. (1975). *Rocks. Sampling and general requirements for the methods of physical testing*. USSR.

[59] State Standard 12730.0-2020. (2020). *Concretes. General requirements for methods of determination of density, moisture content, water absorptions porosity and water tightness*. Kyiv, Ukraine.

[60] State Standard 21153.2-84. (1984). *Rocks. Method for determining the ultimate strength in uniaxial compression*. USSR.

[61] State Standard 21153.7-75. (1975). *Rocks. Method for determining velocities of propagation of elastic longitudinal and transverse waves*. USSR.

[62] Zuievska, N.V. (2012). Change of the hardness characteristics of granite blocks depending on method obtain. *Journal of Donetsk Mining Institute*, *1*(30)-*2*(31), 417-476.

[63] Dong, L., Li, X., Tang, L., & Gong, F. (2011). Mathematical functions and parameters for microseismic source location without pre-measuring speed. *Chinese Journal of Rock Mechanics and Engineering*, *30*, 2057-2067.

[64] Wang, X., Zhao, Y., Gao, Y., Sun, Z., Liu, B., & Jiang, Y. (2023). Energy evolution of anthracite considering anisotropy under high confining pressure: An experimental investigation. *Rock Mechanics and Rock Engineering*, *56*(9), 6735-6759. https://doi.org/10.1007/s00603-023-03398-w

[65] Kong, Y., Zhu, Z.D., & Ruan, H.N. (2018). Stress-seepage coupling characteristics of jointed rock mass under three principal stresses. *Rock and Soil Mechanics*, *39*(6), 2008-2016.

[66] Kong, Y., Ruan, H.N. (2017). Advances in research of coupling characteristics of seepage and stress in rock mass with a single joint. *Journal of Hydroelectric Engineering*, *36*(11), 111-120. https://doi.org/10.11660/slfdxb.20171112

[67] Sun, G.Z., & Lin, W.Z. (1983). The compresstional deformation law of rock mass structure surface and a constitutive equation of rock mass elastic deformation. *Chinese Journal of Geology*, *18*(2), 177-180.

[68] Landau, L.D., & Lifshitz, E.M. (1986). *Theory of elasticity*. Oxford, United Kingdom: Elsevier, 197 p. https://doi.org/10.1016/C2009-0-25521-8

[69] Timoshenko, S., & Goodyear, J.N. (1979). *Theory of elasticity*. Columbus, United States: McGraw Hill Book Company, 560 p.

Дослідження механізму руйнування кристалічного масиву складної будови в умовах трехвісного стискання

О. Іщенко, Л. Новіков, І. Пономаренко, В. Коновал, Р. Кінаш, К. Іщенко

Мета. Експериментальними та теоретичними дослідженнями оцінити характер руйнування зразків тріщинуватого кристалічного масиву складної будови на крихко-пластичній ділянці при їх тривісному навантаженні.

Методика. Для оцінки впливу фізико-механічних властивостей тріщинуватого кристалічного масиву та його структурних особливостей на зміну характеру його руйнування було проведено експериментальні дослідження на зразках гірських порід. Зразки відбиралися у вибоях підготовчих виробок уранових шахт, тунелях метрополітену, що будується (м. Дніпро) та на уступах граніт-них кар'єрів України. Випробування проводилися апробованими методами згідно з чинними державними стандартами. У процесі випробувань зразків і характер формування тріщин оцінювали синхронно мікроскопічним методом скануючим мікроскопом типу GAOSUO P, а їх характеристики – методом акустичної емісії (АЭ) і КТ-сканування промисловим Мікро-КТ сканером, результати яких оброблялись за допомогою ПО Avizo.

Результати. У процесі випробувань зразків було встановлено, що їхня міцність на одновісне стискання та режим руйнування близькі між собою. Випробуваннями виявлено кілька типів кутів нахилу тріщин залежно від напластування. Зі збільшенням значення σ_3 значення σ_{1p} та σ_d практично лінійно збільшуються, а значення σ_{1p} та σ_d зразків спочатку зменшуються, а потім збільшуються зі збільшенням значення β. Встановлено, що між розкриттям тріщини та напруженим станом поверхонь тріщини при навантаженні σ_1 та σ_2 формується додаткова деформація зразка виключно у напрямку σ_3.

Наукова новизна. Встановлено, що при випробуваннях зразків значення σ_3 значно впливає на характеристики діаграми "напруження-деформація" з різними значеннями β. Тоді, збільшення показників σ_3, σ_1-σ_3, ε_1, ε_3, ε_v показує здатність чинити опір при випробуваннях тріщинуватих зразків гірських порід зовнішнім навантаженням і деформаціям. Доведено, що при малому значенні σ_3 лінійна пружна складова дільниці діаграми "напруження-деформація" має більшу частку, ніж дільниці кривої плинності зі збільшенням σ_3.

Практична значимість. Виконані дослідження послужили основою для подальшого розвитку теорії та методів у механіці руйнування тріщинуватого (шаруватого) кристалічного масиву, прогнозування катастроф при веденні гірничих робіт у період будівництва гірничих виробок і тунелів на підприємствах гірничодобувної промисловості.

Ключові слова: *гірська порода; система тривісного навантаження; кристалічний масив; акустична емісія; КТ-сканування; диференціальні напруження*

Publisher's note

All claims expressed in this manuscript are solely those of the authors and do not necessarily represent those of their affiliated organizations, or those of the publisher, the editors and the reviewers.